Anisotropy of spin–orbit induced electron spin relaxation in [001] and [111] grown GaAs quantum dots

2015 New J. Phys. 17 033014

(http://iopscience.iop.org/1367-2630/17/3/033014)

IOP Publishing New J. Phys. 17 (2015) 033014 doi:10.1088/1367-2630/17/3/033014

New Journal of Physics
The open access journal at the forefront of physics

Deutsche Physikalische Gesellschaft DPG
IOP Institute of Physics

Published in partnership with: Deutsche Physikalische Gesellschaft and the Institute of Physics

OPEN ACCESS

RECEIVED
15 October 2014

REVISED
9 February 2015

ACCEPTED FOR PUBLICATION
10 February 2015

PUBLISHED
6 March 2015

PAPER

Anisotropy of spin–orbit induced electron spin relaxation in [001] and [111] grown GaAs quantum dots

C Segarra, J Planelles, J I Climente and F Rajadell

Departament de Química Física i Analítica, Universitat Jaume I, Castelló de la Plana, Spain

E-mail: josep.planelles@uji.es

Keywords: spin–orbit interaction, spin relaxation, quantum dot, magnetic field

Abstract

We report a systematic study of the spin relaxation anisotropy between single electron Zeeman sublevels in three-dimensional cuboidal GaAs quantum dots (QDs). The QDs are subject to an in-plane magnetic field. As the field orientation varies, the relaxation rate oscillates periodically, showing 'magic' angles where the relaxation rate is suppressed by several orders of magnitude. This behavior is found in QDs with different shapes, heights, crystallographic orientations and external fields. The origin of these angles can be traced back to the symmetries of the spin admixing terms of the Hamiltonian. Our results evidence that cubic Dresselhaus terms play an important role in determining the spin relaxation anisotropy, which can induce deviations of the 'magic' angles from the crystallographic directions reported in recent experiments (P Scarlino *et al* 2014 Phys. Rev. Lett. **113** 256802).

1. Introduction

The electron spin confined in semiconductor quatum dots (QDs) is a promising candidate for the realization of quantum computing and the development of spin-based devices in spintronics [1, 2]. Using the spin of electrons as qubits was first proposed by Loss and DiVincenzo [3] and, since then, a lot of effort has been devoted to its accomplishment [4]. QDs offer the possibility of isolating single electron spins which exhibit longer lifetimes than in delocalized systems since quantum confinement suppresses the main bulk decoherence mechanisms [5]. Nevertheless, coupling between the electron spin and the surrounding environment cannot be avoided, resulting in spin relaxation and decoherence. Therefore, a good understanding of the relaxation mechanisms in QDs is needed for the development of spin-based applications.

The two main mechanisms of spin relaxation in III–V zinc-blende semiconductor QDs are the hyperfine coupling with the nuclear spins of the lattice and the spin–orbit interaction (SOI) [4]. The hyperfine interaction is generally important at relatively weak magnetic fields while for moderate and strong fields the phonon-mediated relaxation due to SOI predominates. In semiconductors without inversion symmetry, e.g. GaAs, SOI can be originated by the bulk inversion asymmetry of the material (Dresselhaus SOI) [6] and the structure inversion asymmetry of the confining potential (Rashba SOI) [7]. The Hamiltonians describing both SOI have different symmetries and exhibit an anisotropic behavior [8]. This anisotropy can be exploited to externally control and manipulate the electron spin by changing the orientation of applied magnetic or electric fields [9–11]. As a consequence, the anisotropy of the spin relaxation and its control via external means has been intensively studied [12–20].

Most previous theoretical works have dealt with two-dimensional (2D) circular QDs grown along the [001] crystal direction [4, 12–14, 21], where in-plane anisotropy arises from the interference between Rashba and Dresselhaus SOI. However, QDs are prone to deviate from the circular symmetry and there is gathering evidence that this has a primary influence on the spin relaxation anisotropy [15–18]. This fact has been confirmed in very recent experiments by Scarlino and co-workers [22]. Relevantly, all the studies analyzing the influence of non-circular confinement on the spin relaxation anisotropy of single QDs have so far missed the effect of cubic Dresselhaus SOI terms and that of three-dimensionality (3D). Cubic terms are expected to become particularly

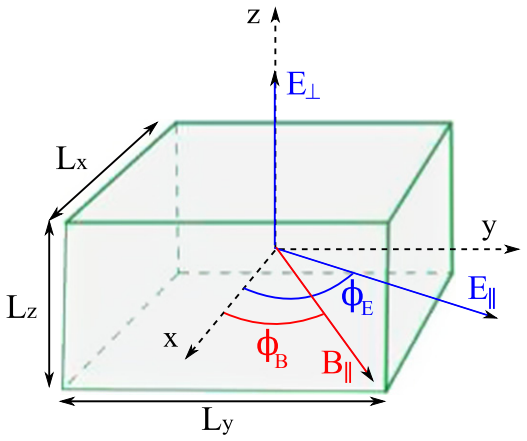

Figure 1. Schematic representation of the cuboidal QD system. The orientation of the external electric and magnetic fields is indicated.

important in tall QDs [23], which are increasingly available owing to recent progress in synthetic control [24, 25]. On the other hand, going beyond [001] grown QDs is also of interest, especially in view of the convenience of [111] grown QDs for optical spin preparation [26]. The effect of the crystallographic orientation on the spin dynamics has been well studied in quantum wells [27–29], but further work is needed in relation to fully localized spins, where studies are limited [18].

In this article, we study the anisotropy of the electron spin relaxation between Zeeman sublevels in cuboidal GaAs QDs. The anisotropy is monitored by varying the orientation of an externally applied in-plane magnetic field (ϕ_B). We consider QDs grown along both [001] and [111] crystal directions, including all linear and cubic terms of Rashba and Dresselhaus SOI in a fully 3D model. Different heights, base shapes, crystallographic orientations, magnetic field intensities and external electric fields are considered. The numerical results, together with perturbative interpretations, provide a wide overview on the effect of confinement asymmetry and 3D on the spin relaxation anisotropy.

We find that, in [001] grown QDs, the spin relaxation anisotropy is very different depending on the dominating spin–orbit mechanism, Rashba or Dresselhaus SOI. By contrast, in [111] grown QDs the anisotropy is the same for both terms. In all cases, the spin relaxation rate shows strong oscillations with ϕ_B. Interestingly, cubic Dresselhaus terms are shown to be critical in determining such anisotropic behavior. This occurs not only in tall QDs, but—contrary to common belief—also in quasi-2D QDs, provided the high symmetry directions of the dot are not aligned with the main crystallographic axes. In both squared and rectangular QDs we observe order-of-magnitude suppressions of the spin relaxation rate at certain 'magic' magnetic field angles ϕ_B, which can be understood from symmetry considerations. A 'magic' angle around [110] has actually been very recently reported in experiments with a single GaAs QD strongly elongated along one in-plane direction [22]. We generalize this study considering less elongated structures. We show that cubic Dresselhaus terms help explain the deviation from [110] observed in the experiment, and in less elongated structures they switch the 'magic' angle to $[\bar{1}10]$ or $[1\bar{1}0]$.

The paper is organized as follows. Section 2 presents the model we use to compute the electron spin relaxation, including the SOI Hamiltonians for QDs rotated with respect to the main crystallographic axes. In section 3 we show and discuss the numerical results for the cases under study. Finally, conclusions are given in section 4.

2. Theoretical model

We study the electron spin relaxation driven by SOI between Zeeman split sublevels of cuboidal GaAs QDs subject to externally applied electric **E** and magnetic **B** fields (see figure 1). The isotropy of the conduction band of III–V semiconductors leads to an isotropic kinetic energy term in the 3D one-electron Hamiltonian which reads

$$H = \frac{\mathbf{p}^2}{2m^\star} + V_c + \mathbf{Er} + H_Z + H_{\mathrm{SOI}}, \tag{1}$$

where $m^\star$ stands for the electron effective mass, V_c is the confinement potential, **E** is an external electric field and $\mathbf{p} = -i\hbar\nabla + \mathbf{A}$, where **A** is the vector potential. An in-plane magnetic field $\mathbf{B} = B\left(\cos\phi_B,\ \sin\phi_B,\ 0\right)$ rotated

an angle ϕ_B with respect to the x axis of the dot is included. This field is described by the vector potential $\mathbf{A} = \left(zB\,\sin\phi_B,\, -zB\,\cos\phi_B,\, 0\right)$. The Zeeman term is $H_Z = \frac{1}{2}g\mu_B\mathbf{B}\boldsymbol{\sigma}$ with g, μ_B and $\boldsymbol{\sigma}$ standing for the electron g-factor, Bohr magneton and Pauli spin matrices, respectively.

The last term in (1) corresponds to the SOI, [8] $H_{\rm SOI} = H_R + H_D$, with H_R being the Rashba SOI

$$H_R^{[001]} = \alpha_r\boldsymbol{\sigma}\left(\mathbf{p}\times\mathbf{E}\right), \tag{2}$$

and H_D the Dresselhaus SOI

$$H_D^{[001]} = \beta_d\Big[\sigma_x p_x\left(p_y^2 - p_z^2\right) + \sigma_y p_y\left(p_z^2 - p_x^2\right) + \sigma_z p_z\left(p_x^2 - p_y^2\right)\Big]. \tag{3}$$

Here, α_r and β_d are material-dependent coefficients determining the strength of the SOI and the superscript [001] indicates de growth direction of the QD.

Equations (2) and (3) correspond to QDs grown along the [001] crystal direction. In order to consider other orientations of the QD with respect to the crystal host we maintain the confinement potential fixed in space and perform a rotation of the crystalline structure. Since the confining potential as well as the externally applied fields are kept while the crystalline structure is rotated, only the $H_{\rm SOI}$ part of the Hamiltonian is affected. In particular, the $H_{\rm SOI}$ Hamiltonian corresponding to an axially applied electric field and a crystalline structure subject to an in-plane rotation θ_z around the z axis reads:

$$H_R^{[001]}\left(\theta_z\right) = \alpha_r E_z\left(\sigma_x p_y - \sigma_y p_x\right), \tag{4}$$

and

$$\begin{aligned} H_D^{[001]}\left(\theta_z\right) = {} & \beta_d\,\cos 2\theta_z\Big[\sigma_x p_x\left(p_y^2 - p_z^2\right) + \sigma_y p_y\left(p_z^2 - p_x^2\right) + \sigma_z p_z\left(p_x^2 - p_y^2\right)\Big] \\ & + \beta_d\,\sin 2\theta_z\Big[p_z^2\left(\sigma_y p_x + \sigma_x p_y\right) - 2\sigma_z p_x p_y p_z + \frac{1}{2}\left(p_x^2 - p_y^2\right)\left(\sigma_x p_y - \sigma_y p_x\right)\Big]. \end{aligned} \tag{5}$$

Note that this particular case of an axially applied electric field yields a Rashba Hamiltonian (4) independent of θ_z.

We consider next QDs grown along the [111] direction. In particular, we consider the rotation $\chi = \arccos\left(1/\sqrt{3}\right)$ around the straight line $y = -x$, that corresponds to the Euler angles $\theta = \arccos\left(1/\sqrt{3}\right)$, $\phi = 45$ and $\alpha = -45$. The rotated SOI Hamiltonians have the form

$$H_R^{[111]} = \frac{\alpha_r E_z}{\sqrt{3}}\Big[\sigma_z\left(p_y - p_x\right) - \sigma_y\left(p_x + p_z\right) + \sigma_x\left(p_y + p_z\right)\Big], \tag{6}$$

and

$$\begin{aligned} H_D^{[111]} = {} & \frac{\beta_d}{2\sqrt{3}}\Big[\left(p_x^2 + p_y^2 - 4p_z^2\right)\left(p_x\sigma_y - p_y\sigma_x\right) + p_z\left(p_x^2 - p_y^2\right)\left(\sigma_x + \sigma_y\right) \\ & + 2p_x p_y p_z\left(\sigma_x - \sigma_y\right) - \sigma_z p_x^2\left(p_x + 3p_y\right) + \sigma_z p_y^2\left(p_y + 3p_x\right)\Big], \end{aligned} \tag{7}$$

where the electric field is aligned with the dot z axis.

The relaxation rate between the initial electron state $|\Psi_i\rangle$ and the final electron state $|\Psi_f\rangle$ is estimated by the Fermi golden rule

$$\frac{1}{T_1} = \frac{2\pi}{\hbar}\sum_{\lambda,\mathbf{q}}\left|M_\lambda\left(\mathbf{q}\right)\right|^2\left|\left\langle\Psi_f\left|\mathrm{e}^{-\mathrm{i}\mathbf{q}\mathbf{r}}\right|\Psi_i\right\rangle\right|^2\delta\left(E_f - E_i - E_q\right). \tag{8}$$

Here, the sum is done over all possible decay channels and directions of the phonon wave vector $\mathbf{q}$. $M_\lambda\left(\mathbf{q}\right)$ denotes the scattering matrix element corresponding to the electron–phonon interaction including the piezoelectric and deformation potentials [30]. The expressions for $M_\lambda\left(\mathbf{q}\right)$ are derived considering the three phonon modes λ of the bulk zinc-blende crystals, one longitudinal and two transversals, as producing strain and this strain yielding piezoelectricity (see [31] for more details). We assume bulk phonons, which is an appropiate model for embedded QDs. As a consequence, the scattering matrix elements $M_\lambda\left(\mathbf{q}\right)$ does not depend on the QD orientation. All calculations are carried out at zero temperature, thus only phonon emission processes are possible, i.e. those inducing transitions from the first excited to the ground electronic state. The splitting energy between Zeeman sublevels is small so that only acoustic phonons are important and the linear dispersion regime applies $E_q = \hbar c_\lambda q$, where c_λ is the velocity of the longitudinal or transversal phonon branch [32]. Note that phonons cannot couple states with opposite spin and the spin admixture caused by SOI is essential for relaxation to take place.

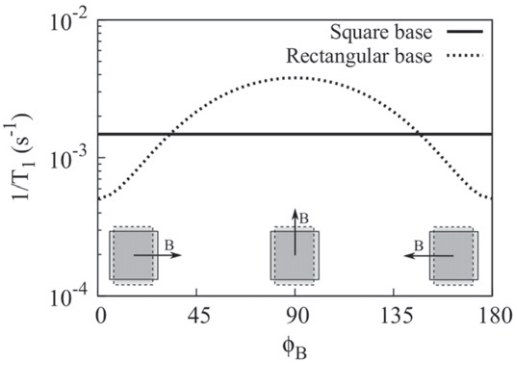

Figure 2. Electron spin relaxation rate as a function of the in-plane magnetic field orientation when only the Rashba SOI contribution is included. QDs of 10 nm height with rectangular (dotted line) and square base (solid line) are considered.

The eigenvalue problem is solved numerically using a finite difference method on a 3D grid. Accounting for SOI in the calculation of the energy spectra requires high numerical precision due to the small magnitude of this coupling and the presence of third-order derivatives. Accuracy in the derivatives in the finite difference method can be achieved by increasing the number of mesh nodes. However, the 3D character of the calculations is a serious hindrance, since the number of nodes increases as $n_x \cdot n_y \cdot n_z$, with n_i the discretization along the axis i. We can also improve accuracy by increasing the points of the discretization of derivatives. We have explored the performance of 5, 7 and 15-point central difference schemes and, after a series of convergence tests, found that a seven-point stencil central difference scheme and a number of 42875 mesh nodes discretizing the 3D system guarantees an appropiate description at a reasonable computational cost. In order to preserve the accuracy we model QDs as hard-wall cuboids fitting exact numbers of nodes, so that the potential energy term does not introduce any additional inaccuracy. This idealized geometry has been shown to capture the basic features of the spin–orbit anisotropy of realistic InAs/GaAs QDs [11], while enabling a simple interpretation in terms of symmetries, which is the goal of this work.

We use GaAs material parameters, particularly electron effective mass $m^\star = 0.067$, density $\rho = 5310$ kg m^{-3}, dielectric constant $\epsilon_r = 12.9$, piezoelectric constant $h_{14} = 1.45 \times 10^9$ V m^{-1}, g-factor $g = -0.44$ and sound velocities $c_l = 4720$ m s^{-1} and $c_t = 3340$m s^{-1}. [33, 34] For the SOI constants, we take $\beta_d = 27.58eV$ Å^3 and $\alpha_r = 5.026e$Å^2. [8] All simulations are carried out, unless otherwise stated, considering an axial electric field $E_z = 10$ kV cm^{-1} and an in-plane magnetic field $B_\parallel = 1\ T$.

3. Results and discussion

3.1. Geometry dependence

We investigate first the relaxation rate anisotropy for different dot geometries when applying an in-plane magnetic field at different orientations. The QDs considered have a base with square ($L_x = 80nm, L_y = 80$ nm) or rectangular ($L_x = 70$ nm, $L_y = 90$ nm) shape and various heights ranging from $L_z = 10$ nm to $L_z = 40$ nm.

Figure 2 shows the spin relaxation rate when only Rashba SOI is present. .[1] For QDs with square base the relaxation rate is constant for any ϕ_B. In contrast, in rectangular QDs it presents an anisotropic behavior, where the maximum (minimum) corresponds to a magnetic field oriented along the direction of weaker (stronger) confinement. In both cases, $1/T_1$ is independent of the QD height and, for the sake of clarity, only results for $L_z = 10nm$ are included in figure 2.

In figure 3(a), we analyze the spin relaxation in the only presence of Dresselhaus SOI for QDs with square base. The relaxation rate for short QDs ($L_z = 10$ nm) is almost isotropic with the orientation of the magnetic field. This is in sharp contrast with taller QDs, where strong quenchings are found at $\phi_B = 45$ and $\phi_B = 135$. On the other hand, when the QD base is rectangular, figure 3(b), only moderate modulations of $1/T_1$ are observed. Again, the dependence on ϕ_B is different depending on the dot height. When $B_\parallel$ is oriented along the direction of weaker confinement the relaxation is minimum for QDs with $L_z = 10$ nm, but it changes into a maximum for $L_z = 20,\ 30,\ 40$ nm.

[1] The relaxation is slower than in previous studies (e.g. [14, 21]) because in our cuboidal QDs there is no potential gradient, so the only source of inversion asymmetry contributing to equation (2) is the (relatively weak) external field **E**. The dependence on ϕ_B we describe below is however largely independent of the strength of the field

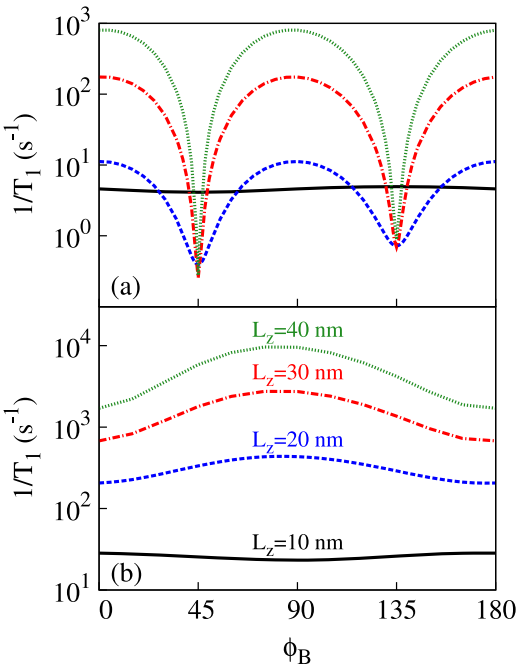

Figure 3. Calculated spin relaxation rate versus magnetic field orientation ϕ_B considering only Dresselhaus SOI in (a) square and (b) rectangular base QDs. Different dot heights are studied: $L_z = 10$ *nm* (solid black line), $L_z = 20$ *nm* (blue dashed line), $L_z = 30$ *nm* (red dash-dotted line) and $L_z = 40$ *nm* (green dotted line).

The preceding results reveal a strong sensitivity of the spin relaxation anisotropy to both the QD symmetry (squared or rectangular) and the QD height. Both factors can induce major, qualitative changes in the anisotropy. To understand such a behavior, we consider that the relaxation rate is proportional to the degree of spin admixture of the initial and final states of the transition, Ψ_i and Ψ_f in (8) [32]. These states can be approximated as:

$$\Psi_i \approx \psi_{000}|\downarrow\rangle + c_x^i\psi_{100}|\uparrow\rangle + c_y^i\psi_{010}|\uparrow\rangle$$
$$\Psi_f \approx \psi_{000}|\uparrow\rangle + c_x^f\psi_{100}|\downarrow\rangle + c_y^f\psi_{010}|\downarrow\rangle, \quad (9)$$

where ψ_{ijk} represents the electron orbital in the absence of SOI, with ijk the number of nodes in x, y and z, respectively, while $|\uparrow\rangle$ ($|\downarrow\rangle$) represents parallel (antiparallel) spin alignment along the direction of the magnetic field. For the analysis we can focus on Ψ_i (analogous reasoning is valid for Ψ_f). Ψ_i is mostly a spin down state, with a little SOI induced spin admixture with excited levels. Notice that $\psi_{000}|\uparrow\rangle$ does not contribute to the spin admixture of Ψ_i because the parity symmetry in x and y prevents direct SOI coupling with $\psi_{000}|\downarrow\rangle$. Thus, the degree of spin admixture is essentially captured by the coefficients c_x^i and c_y^i, which can be estimated perturbatively as:

$$c_x^i = -\frac{\langle\uparrow|\langle\psi_{100}|H_{SOI}|\psi_{000}\rangle|\downarrow\rangle}{\varepsilon_{100\uparrow} - \varepsilon_{000\downarrow}}, \quad (10)$$

and

$$c_y^i = -\frac{\langle\uparrow|\langle\psi_{010}|H_{SOI}|\psi_{000}\rangle|\downarrow\rangle}{\varepsilon_{010\uparrow} - \varepsilon_{000\downarrow}}. \quad (11)$$

The energy separations $\Delta\varepsilon_x = \varepsilon_{100\uparrow} - \varepsilon_{000\downarrow}$ and $\Delta\varepsilon_y = \varepsilon_{010\uparrow} - \varepsilon_{000\downarrow}$ do not vary with ϕ_B. Thus, the origin of the anisotropy must be sought in the SOI matrix elements.

We consider first Rashba SOI, i.e. $H_{SOI} = H_R^{[001]}(0)$. From (4) and parity considerations, it follows that, for $\phi_B = 0$,

$$c_x^i = \alpha_r E_z \frac{\langle\uparrow|\sigma_y|\downarrow\rangle\langle\psi_{100}|p_x|\psi_{000}\rangle}{\Delta\varepsilon_x}, \qquad c_y^i = 0 \quad (12)$$

while for $\phi_B = 90$,

$$c_x^i = 0, \qquad c_y^i = \alpha_r \, E_z \frac{\left\langle \uparrow \left| \sigma_x \right| \downarrow \right\rangle \left\langle \psi_{010} \left| p_y \right| \psi_{000} \right\rangle}{\Delta\varepsilon_y}. \tag{13}$$

We see that depending on the orientation of the magnetic field the spin admixture is caused by the coupling to a different excited state. For QDs with square base $\Delta\varepsilon_x = \Delta\varepsilon_y$, and $\langle\psi_{100}|\, p_x \,|\psi_{000}\rangle = \langle\psi_{010}|\, p_y |\psi_{000}\rangle$. Consequently, the degree of spin mixing does not change at $\phi_B = 0$ and $\phi_B = 90$, in agreement with the isotropic $1/T_1$ observed in figure 2. Conversely, in rectangular QDs with stronger confinement in x, $\Delta\varepsilon_x > \Delta\varepsilon_y$. Then, the admixture coefficients at $\phi_B = 90$ are larger than at $\phi_B = 0$, which justifies the anisotropy observed in figure 2.

The anisotropy of Dresselhaus SOI induced spin relaxation, shown in figure 3, can be understood in similar terms. We split equation (3) as $H_D^{[001]} = H_z + H_{xy}$, where $H_z = \beta_d p_z^2 \left(p_y \sigma_y - p_x \sigma_x \right)$ and $H_{xy} = H_x + H_y = \beta_d \left[p_x^2 \left(p_z \sigma_z - p_y \sigma_y \right) + p_y^2 \left(p_x \sigma_x - p_z \sigma_z \right) \right]$. Calculations using these Hamiltonians independently show that H_z dominates for $L_z = 10\ nm$, in agreement with the usual practice of approximating the Dresselhaus SOI by H_z in quasi-2D systems. If we perform a similar analysis for H_z as the one carried out for Rashba SOI, we find that coupling to ψ_{010} and ψ_{100} dominates at $\phi_B = 0$ and $\phi_B = 90$, respectively. This is exactly the opposite as for the Rashba SOI case, explaining the results obtained for $L_z = 10\ nm$ QDs (see figure 3(b)). As the QD height is increased, however, H_{xy} soon dominates over H_z. Indeed, for $L_z = 20\ nm$ it is already dominant. Considering individually H_x and H_y it can be shown that they present opposite behaviors with ϕ_B. H_x produces a maximum (minimum) relaxation for $\phi_B = 90$ ($\phi_B = 0$) and H_y for $\phi_B = 0$ ($\phi_B = 90$). This dependence does not change with the base shape and a stronger confinement in one direction only determines which term, H_x or H_y, prevails. In the rectangular dot of figure 3(b), $L_x < L_y$ so H_x is more important and we observe its angular dependence. Instead, when the dot base is squared H_x and H_y cancel each other out at $\phi_B = 45$ and $\phi_B = 135$, thus giving rise to the pronounced minima of $1/T_1$ observed in figure 3(a).

To summarize this section, the spin relaxation anisotropy of [001] grown GaAs QDs is determined by the spin admixture induced by SOI. This is qualitatively different in systems where Rashba or Dresselhaus SOI terms dominate. In the latter case, the anisotropy reflects whether H_z or H_{xy} prevails. It turns out that H_{xy} is already dominant for $L_z = 20\ nm$ (height-to-base aspect ratio of 1:4), which points out at the early relevance of cubic Dresselhaus terms in structures where 3D starts becoming important. In this case, the use of QDs with symmetric x–y confinement enables strong suppressions of the relaxation at certain magnetic field orientations.

3.1.1. The influence of strong magnetic fields

We study next the spin relaxation angular dependence in square QDs under strong magnetic fields. In such a case, the orbital effects of the magnetic field are expected to play an important role, especially in tall systems. We emphasize the need of a true 3D calculation to account for this effect, since it cannot be properly described using 2D models [14]. We calculate the relaxation rate for different values of the magnetic field up to $B_\parallel = 10T$ in QDs with $L_x = L_y = 80\ nm$ and $L_z = 20\ nm$.

The impact of the magnetic field strength on the angular dependence through the Rashba SOI is negligible and not shown. We enclose in figure 4 the spin relaxation yielded by the Dresselhaus SOI term only. Figure 4 shows that the minima of $1/T_1$ at $\phi_B = 45$ and $\phi_B = 135$ is gradually removed for strong magnetic fields. This behavior can be understood in terms of the differential contribution of H_{xy} and H_z, as pointed out previously. For QDs with $L_z = 20\ nm$ and $B_\parallel = 1T$, H_{xy} dominates and we observe two pronounced minima (see inset in figure 4). When $B_\parallel$ increases, H_z rises up and it becomes dominant at $B_\parallel = 10T$, this being responsible for the suppression of the minima. It is noteworthy to mention that an increase in the height of the dot enhances the effects of the magnetic field but also diminishes the contribution of H_z to the Hamiltonian. As a consequence, in taller QDs a balance of these two contributions will determine which term, H_{xy} or H_z, dominates and, therefore, the angular dependence of the spin relaxation.

3.2. In-plane confinement potential orientation

In this section, we investigate the impact of the QD orientation with respect to the crystal host on the spin relaxation. The rotation angle θ_z is defined as the angle between the [001] crystal direction and the x axis of the dot, see inset of figure 5(a) for a schematic representation. All calculations are carried out with the magnetic field $B_\parallel = 1T$ oriented along the x axis of the QD and an axial electric field $E_z = 10$ kV cm^{-1}.

In figure 5(a), we plot the relaxation rate in the presence of Rashba SOI only for QDs with $L_z = 10\ nm$ (results for $L_z = 20\ nm$ are identical and are omitted for clarity). We find that $1/T_1$ is not affected by changes in the dot orientation. This result is as expected since (4) does not depend on θ_z.

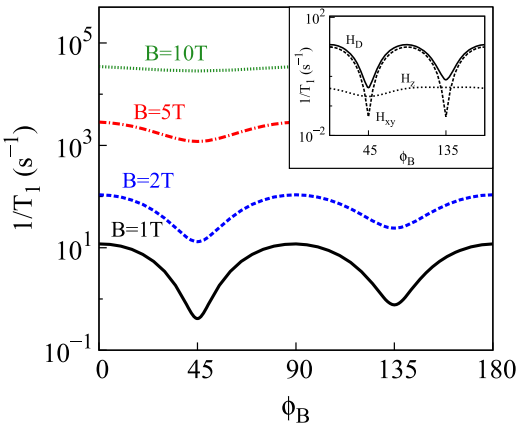

Figure 4. Spin dynamics of a square QD of $L_z = 20\ nm$ as a function of ϕ_B for different magnetic field intensities: $B_{\|} = 1T$ (black solid line), $B_{\|} = 2T$ (blue dashed line), $B_{\|} = 5T$ (red dash-dotted line) and $B_{\|} = 10T$ (green dotted line). Only the presence of Dresselhaus SOI is considered. The inset shows the spin relaxation for $B_{\|} = 1T$ when considering the full Dresselhaus Hamiltonian $H_D = H_{xy} + H_z$ (solid line), and also the partial contributions of H_{xy} (dashed line) and H_z (dotted line).

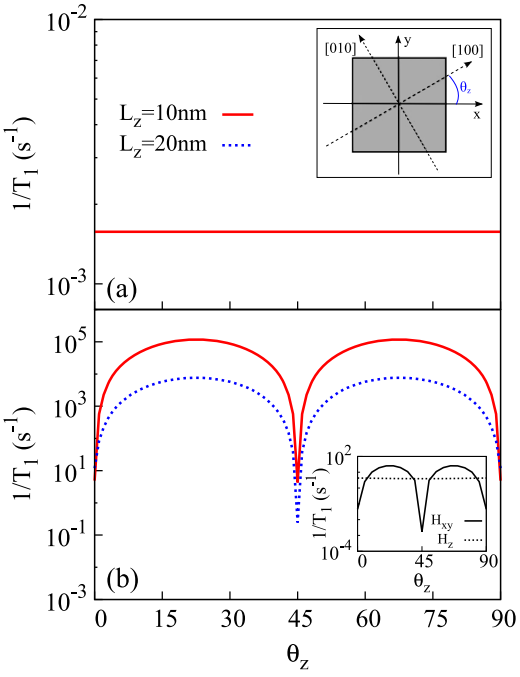

Figure 5. Spin relaxation rate as a function of the dot orientation θ_z for square base QDs with $L_z = 10\ nm$ (black solid curve) and $L_z = 20\ nm$ (blue dotted curve). Results are shown for (a) pure Rashba SOI and (b) pure Dresselhaus SOI. The in-plane magnetic field $B_{\|} = 1T$ is oriented along the dot x axis ($\phi_B = 0$). The inset in (a) illustrates a representation of the system and the definition of the rotation angle. The inset in (b) shows the relaxation due to H_{xy} and H_z in the $L_z = 10\ nm$ dot.

For the Dresselhaus SOI case instead, figure 5(b) shows a strong dependence of $1/T_1$ on the confinement potential rotation. In particular, one can see some specific rotation angles, $\theta_z = 0,\ 45,\ 90$, where the spin relaxation is reduced by 4–5 orders of magnitude as compared to others. This behavior can be understood from the form of the Hamiltonian in (5). The Dresselhaus SOI presents a $2\theta_z$ dependence, with half of the terms multiplied by $\sin 2\theta_z$ and the other half by $\cos 2\theta_z$. Therefore, the first part of (5) cancels for $\theta_z = 45$ and the second part for $\theta_z = 0$ and $\theta_z = 90$. This suppresses some of the SOI coupling channels, giving rise to slower relaxation rates than for intermediate angles.

It is noteworthy to mention that the dependence on θ_z originates in H_{xy}, with H_z remaining isotropic, see figure 5(b) inset. This highlights the important role of the cubic terms of the Dresselhaus SOI Hamiltonian in GaAs QDs. As a matter of fact, the inset shows that even in the shortest QDs ($L_z = 10\ nm$), save for the vicinity of

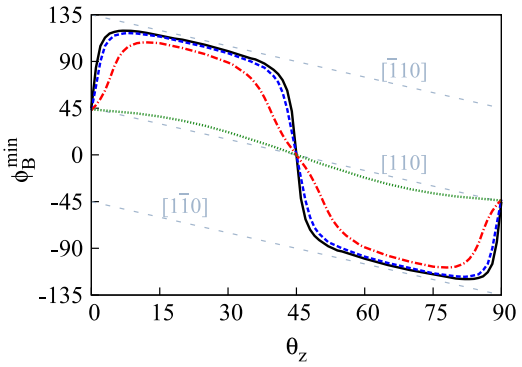

Figure 6. 'Magic' angle as a function of the dot orientation θ_z for a QD with $L_z = 10\ nm$, $L_x = 80\ nm$ and various L_y: $L_y = 80\ nm$ (black solid line), $L_y = 90\ nm$ (blue dashed line), $L_y = 110\ nm$ (red dash-dotted line) and $L_y = 150\ nm$ (green dotted line). The grey dashed lines correspond to ϕ_B pointing along [110], [$\bar{1}$10] and [1$\bar{1}$0] direction for each θ_z.

the 'magic' rotation angles ($\theta_z = 0,\ 45,\ 90$) the main contribution to the relaxation rate does not come from H_z but from H_{xy}.

These results are robust against changes in the QD geometry, such as height and base shape, which do not modify the qualitative trend. In particular, the minimum at $\theta_z = 45$ remains unaltered while the minima at $\theta_z = 0$ and $\theta_z = 90$ are only slightly shifted in rectangular QDs.

Recent experiments by Scarlino and co-workers have also explored spin relaxation anisotropy of GaAs QDs. [22] For their specific QD, they observed a periodicity of 180 degrees in ϕ_B, with a 'magic' angle near [110]. Both the periodicity and the relaxation suppression were explained assuming Rashba and Dresselhaus SOI terms had roughly the same weight and the QD was strongly elongated in one direction. It was shown that the deviation from the [110] direction could arise from the values of θ_z and the Rashba to Dresselhaus SOI strength ratio, which are unknown for their sample. Here we generalize this study by considering QDs with different in-plane shape, from square (L_x=L_y) to strongly elongated ($L_x \ll L_y$), and include the cubic Dresselhaus terms which are missing in their analysis. We set Rashba SOI to be as strong as the linear (H_z) Dresselhaus term by setting $\alpha_r = \beta_d \langle p_z^2 \rangle / E_z$. The results are shown in figure 6.

One can see that for the strongly elongated QD, $L_y = 150nm$, the 'magic' angle $\phi_B^{\min}$ takes place when the magnetic field points approximately along [110] ($\phi_B^{\min} \simeq 45 - \theta_z$). This is consistent with the estimates of Scarlino *et al* (figure 4(a) in [22]). The small deviations from [110] (dashed grey line in figure 6) are atributed to the influence of the cubic Dresselhaus terms. As the QD elongation is reduced, the anisotropy evolves towards a completely different limit, which is reached for the square QD, $L_y = 80nm$. In this case, the magic angle remains at [110] for $\theta_z = 0,\ 45,\ 90$, but it rapidly deviates for any other θ_z. For $0 < \theta_z < 45$ it switches to [$\bar{1}$10] ($\phi_B^{\min} \simeq 135 - \theta_z$), while for $45 < \theta_z < 90$ it switches to [1$\bar{1}$0] ($\phi_B^{\min} \simeq -45 - \theta_z$). The origin of this distinct behavior is the same discussed in figure 5(b) inset. Namely, when the x axis of the dot does not coincide with [100], [110] or [010], Dresselhaus H_{xy} terms take over H_z ones. This breaks the balance between Rashba and H_z Dresselhaus SOI described in [22]. Because statistically QDs are likely to be tilted from $\theta_z = 0,\ 45,\ 90$, it follows that cubic Dresselhaus terms can induce severe deviations from the spin–orbit anisotropy described in the experiment if the QDs are not strongly elongated.

3.3. Effect of an additional in-plane electric field

We next explore the influence of applying an in-plane electric field on the spin relaxation anisotropy. We consider the squared QD of section 3.1 with $B_\parallel = 1T$ and $E_z = 10$ kV cm^{-1}, but now we add an additional electric field component $E_\parallel = 10kV\ cm^{-1}$. Calculations are performed rotating the in-plane electric field for some fixed magnetic field orientations.

In figures 7(a) and (b), we present the relaxation rate obtained for pure Rashba and pure Dresselhaus SOI, respectively, at four different ϕ_B values. The most remarkable finding is that $1/T_1$ is increased by several orders of magnitude in comparison with the case with only axial electric field (figures 2 and 3), although strong suppressions show up at some specific combinations of ϕ_B and ϕ_E. For Rashba SOI the combination is $\phi_B - \phi_E = 90,\ 270$ and for Dresselhaus SOI $\phi_B + \phi_E = 0,\ 180$. Changes in the QD geometry do not modify significantly the qualitative results shown in figure 7. Only small displacements of the cancellation angles and the moderation of some minima occur.

The influence of the in-plane electric field can be explained from the fact that $E_\parallel$ breaks the parity symmetry in the direction ϕ_E. This enables the otherwise forbidden SOI coupling between the Zeeman sublevels $\psi_{000}|\uparrow\rangle$

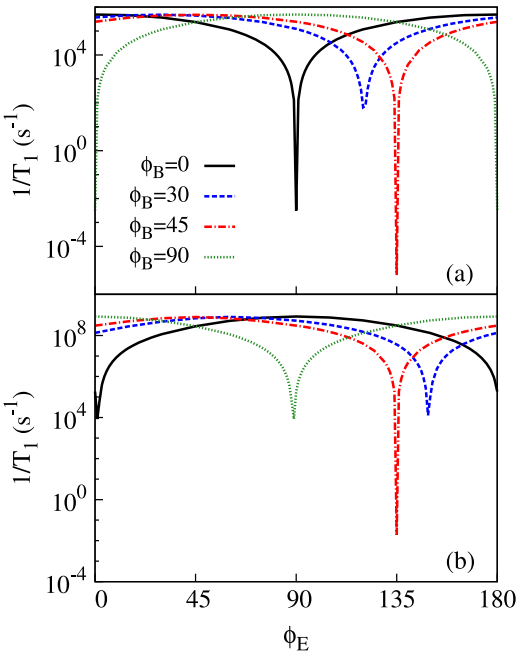

Figure 7. Electron spin relaxation as a function of the in-plane electric field orientation ϕ_E considering (a) only Rashba SOI and (b) only Dresselhaus SOI. The QDs studied have square base and $L_z = 10$ *nm*. Calculations with the magnetic field oriented at some fixed angles are presented: $\phi_B = 0$ (black solid line), $\phi_B = 30$ (blue dashed line), $\phi_B = 45$ (red dash-dotted line) and $\phi_B = 90$ (green dotted line).

and $\psi_{000}|\downarrow\rangle$ in Ψ_i and Ψ_f (recall section 3.1). Since these states are very close in energy, the ensuing spin admixture is important, which justifies the large enhancement of $1/T_1$. In order to understand the minima we carry out a similar perturbative analysis to that of section 3.1 but now focusing on the coupling between the two ψ_{000} sublevels. Let us consider first the Dresselhaus SOI term. Assuming $H_D^{[001]} \approx H_z$ (as is the case for quasi-2D QDs and $\theta_z = 0$), the $\phi_B = 0$ matrix element is:

$$\left\langle \psi_{000}\left\langle \uparrow \left| H_z \right| \psi_{000} \right| \downarrow \right\rangle = \beta_d \left\langle \downarrow \left| \sigma_y \right| \uparrow \right\rangle \left\langle \psi_{000} \left| p_z^2\, p_y \right| \psi_{000} \right\rangle. \tag{14}$$

The integral of the orbital part in (14) vanishes when $\phi_E = 0$ because of the odd parity along y, but other orientations of the electric field break the parity symmetry in the y direction and then $1/T_1$ increases, as seen in figure 7(b) (black line). Similar reasoning shows that for $\phi_B = 90$ the parity-induced minimum occurs at $\phi_E = 90$. For intermediate magnetic field angles, however, the minimum no longer takes place when $E_\parallel \parallel \mathbf{B}$. Indeed, for $\phi_B = 45$, the minimum is found at $\phi_E = 135$ ($E_\parallel \perp \mathbf{B}$). To explain this, it is convenient to rotate the coordinate system 45 degrees from (x,y) into (x', y') so that the x′ axis is aligned with the direction of **B**. As inferred from (5), the resulting SOI term is $H_z^{45} = \beta_d p_z^2 (\sigma_{y'} p'_x + \sigma_{x'} p'_y)$ and the matrix element becomes:

$$\left\langle \psi_{000}\left\langle \uparrow \left| H_z^{45} \right| \psi_{000} \right| \downarrow \right\rangle = \beta_d \left\langle \downarrow \left| \sigma_{y'} \right| \uparrow \right\rangle \left\langle \psi_{000} \left| p_z^2\, p'_y \right| \psi_{000} \right\rangle. \tag{15}$$

This integral vanishes due to the odd parity in x′ when $E_\parallel$ is parallel to the y′ axis, i.e. when $\phi_E = 135$ in the initial coordinate frame, in agreement with figure 5(b).

The minima in the presence of Rashba SOI can be explained in similar terms, but because $H_R^{[001]}$ has rotational symmetry, see equation (4), it does not change when rotating the coordinate system. Then, the minima always take place for $E_\parallel \perp \mathbf{B}$.

To summarize this section, the presence of in-plane electric fields greatly enhances spin relaxation due to the lowered orbital symmetry, but the anisotropy of both Rashba and Dresselhaus SOI makes it possible to find relative angles between $E_\parallel$ and **B** such that the relaxation is severely reduced.

3.4. [111] Grown QDs

In figure 8 we plot the spin relaxation rate for the squared QD studied in section 3.1, but now considering the dot is grown along the [111] crystal direction. In general, faster relaxation rates are obtained for this orientation as compared to the [001] grown QDs. Interestingly, we observe the same angular dependence for both Rashba SOI (figure 8(a)) and Dresselhaus SOI (figure 8(b)). Both mechanisms show strong suppressions at $\phi_B = 135$ and $\phi_B = 315$. However, when increasing L_z Rashba and Dresselhaus SOI mechanisms show opposite behaviors and

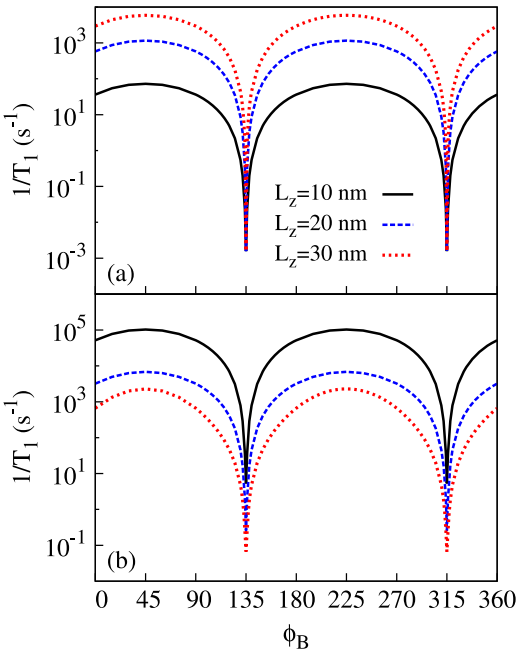

Figure 8. Electron spin dynamics of square QDs grown along the [111] crystallographic direction as a function of the magnetic field orientation. Simulations considering (a) the Rashba SOI and (b) the Dresselhaus SOI are included for three QD heights: $L_z = 10$ *nm* (black solid curve), $L_z = 20$ *nm* (blue dashed curve) and $L_z = 30$ *nm* (red dotted curve).

$1/T_1$ increases and decreases, respectively. Therefore, the dot height determines which of the coupling mechanisms dominates.

The cancellation angles of the relaxation in figure 8 can be justified noting that the canonical momenta $p_x = -i\hbar \mathrm{d}/\mathrm{d}_x + zB \sin \phi_B$ and $p_y = -i\hbar \mathrm{d}/\mathrm{d}_y - zB \cos \phi_B$ have exactly the same form for $\phi_B = 135$ and $\phi_B = 315$ since $L_x = L_y$. As a result, the first term in (6) and several terms in (7) cancel out, yielding two sharp minima in the scattering rate curve.

The identical anisotropy of Rashba and Dresselhaus SOI induced spin relaxation in [111] QDs revealed by figure 8, which is a consequence of the formal equivalences between $H_R^{[111]}$ and $H_D^{[111]}$, [35], facilitates in practice the simultaneous quenching of both mechanisms. For magnetic fields where hyperfine interaction is negligible and square dots, this should lead to spin lifetimes in the range of seconds. We have further checked that changes in the QD base shape do not modify the qualitative behavior reported above, the minima being only slightly shifted for rectangular dots under Dresselhaus SOI.

4. Conclusions

We have investigated systematically the electron spin scattering anisotropy in 3D cuboidal GaAs QDs grown along the [001] and [111] directions. We have shown that the relaxation rate can be controlled by several orders of magnitude by varying the in-plane orientation of external magnetic and electric fields.

In [001] grown QDs under an axial electric field, the spin relaxation in-plane anisotropy is strongly dependent on the QD geometry and the nature of the dominating SOI term. For Rashba SOI, the relaxation is isotropic or anisotropic when the base is squared and rectangular, respectively, and it is not affected by changes in the QD height. On the other hand, for Dresselhaus SOI, the relaxation presents a different behavior depending not only on the base shape, but also on the QD height. In fact, short and tall dots can even show contrary angular dependence, evidencing the important role of QD 3D. In addition, we have demonstrated that the isotropic/anisotropic behavior can be controlled by changing the magnetic field strength.

We have also shown that rotating the confinement potential in-plane with respect to the crystal structure causes an important modulation of the spin relaxation, that is severely suppressed when the high symmetry directions of the QD confinement match the main crystallographic axes. This modulation arises from the cubic Dresselhaus terms, which are important even for small heights. Such terms can explain the deviation of the slow spin relaxation direction of the magnetic field away from [110], as measured in very recent experiments [22], for strongly elongated QDs. For less elongated structures they can even switch it to $[1\bar{1}0]$ or $[\bar{1}10]$.

An additional in-plane electric field component causes a strong increase in the relaxation rate, but certain combinations of ϕ_B and ϕ_E lead to enhanced spin lifetimes. We find that these combinations are different for Rashba, $\phi_B - \phi_E = 90,\ 270$, and Dresselhaus SOI, $\phi_B + \phi_E = 0,\ 180$.

We have further studied QDs grown along the [111] direction. We have found that Rashba and Dresselhaus SOI present the same angular dependence with ϕ_B, with pronounced minima at certain magnetic field orientations. This enables simultaneous suppression of Rashba and Dresselhaus SOI induced spin relaxation, which is an advantadge as compared to more conventional [001] grown QDs.

Acknowledgments

This work was supported by UJI-Bancaixa Project No. P1-1B2011-01, MINECO Project No. CTQ2011-27324, and FPU Grant (C S).

References

[1] Awschalom D D, Loss D and Samarth N 2002 *Semiconductor Spintronics and Quantum Computation* (Berlin: Springer)
[2] Fabian J, Matos-Abiague A, Ertler C, Stano P and Žutić I 2007 *Acta Phys. Slovaca* **57** 565
[3] Loss D and DiVincenzo D P 1998 *Phys. Rev.* A **57** 120
[4] Hanson R, Kouwenhoven L P, Petta J R, Tarucha S and Vandersypen L M K 2007 *Rev. Mod. Phys.* **79** 1217
[5] Khaetskii A V and Nazarov Y V 2000 *Phys. Rev.* B **61** 12639
[6] Dresselhaus G 1955 *Phys. Rev.* **100** 580
[7] Bychkov Y A and Rashba E I 1984 *J. Phys.* C **17** 6039
[8] Winkler R 2003 *Spin-Orbit Coupling Effects in Two-Dimensional Electron and Hole Systems* (Berlin: Springer)
[9] Könemann J, Haug R J, Maude D K, Fal'ko V I and Altshuler B L 2005 *Phys. Rev. Lett.* **94** 226404
[10] Takahashi S, Deacon R S, Yoshida K, Oiwa A, Shibata K, Hirakawa K, Tokura Y and Tarucha S 2010 *Phys. Rev. Lett.* **104** 246801
[11] Nowak M P and Szafran B 2013 *Phys. Rev.* B **87** 205436
[12] Fal'ko V I, Altshuler B L and Tsyplyatyev O 2005 *Phys. Rev. Lett.* **95** 076603
[13] Destefani C F and Ulloa S E 2005 *Phys. Rev.* B **72** 115326
[14] Stano P and Fabian J 2006 *Phys. Rev. Lett.* **96** 186602
[15] Olendski O and Shahbazyan T V 2007 *Phys. Rev.* B **75** 041306
[16] Amasha S, MacLean K, Radu I P, Zumbühl D M, Kastner M A, Hanson M P and Gossard A C 2008 *Phys. Rev. Lett.* **100** 046803
[17] Prabhakar S, Melnik R and Bonilla L L 2013 *Phys. Rev.* B **87** 235202
[18] Stano P and Fabian J 2006 *Phys. Rev.* B **74** 045320
[19] Nowak M P, Szafran B, Peeters F M, Partoens B and Pasek W J 2011 *Phys. Rev.* B **83** 245324
[20] Stepanenko D, Rudner M, Halperin B I and Loss D 2012 *Phys. Rev.* B **85** 075416
[21] Golovach V N, Khaetskii A and Loss D 2004 *Phys. Rev. Lett.* **93** 016601
[22] Scarlino P, Kawakami E, Stano P, Shafiei M, Reichl C, Wegscheider W and Vandersypen L M K 2014 *Phys. Rev. Lett.* **113** 256802
[23] Planelles J, Climente J I and Segarra C 2012 *J. Phys. Chem.* C **116** 25143
[24] Dalacu D, Mnaymneh K, Wu X, Lapointe J, Aers G C, Poole P J and Williams R L 2011 *Appl. Phys. Lett.* **98** 251101
[25] Pfund A, Shorubalko I, Leturcq R and Ensslin K 2006 *Appl. Phys. Lett.* **89** 252106
[26] Mano T, Abbarchi M, Kuroda T, McSkimming B, Ohtake A, Mitsuishi K and Sakoda K 2010 *Appl. Phys. Express* **3** 065203 and references therein
[27] Vurgaftman I and Meyer J R 2005 *J. Appl. Phys.* **97** 053707
[28] Biermann K, Hernández-Mínguez A, Hey R and Santos P V 2012 *J. Appl. Phys.* **112** 083913
[29] Balocchi A, Amand T, Wang G, Liu B L, Renucci P, Duong Q H and Marie X 2013 *New J. Phys.* **15** 095016
[30] Climente J I, Bertoni A, Goldoni G and Molinari E 2006 *Phys. Rev.* B **74** 035313
[31] Climente J I, Segarra C and Planelles J 2013 *New J. Phys.* **15** 093009
[32] Khaetskii A V and Nazarov Y V 2001 *Phys. Rev.* B **64** 125316
[33] Vurgaftman I, Meyer J R and Ram-Mohan L R 2001 *J. Appl. Phys.* **89** 5815
[34] Madelung O (ed) 1982 *Semiconductors. Physics of Group IV Elements and III–V Compounds* (*Landolt–Börnstein* vol 17) (Berlin: Springer)
[35] Žutić I, Fabian J and Das Sarma S 2004 *Rev. Mod. Phys.* **76** 323